Landes Bioscience

www.landesbioscience.com

Supplemental Material to:

Leonid E. Fridlyand, David A. Jacobson, L.H. Philipson

Ion channels and regulation of insulin secretion in human β cells: A computational systems analysis

Islets 2012; 5(1)
http://dx.doi.org/10.4161/isl.24166

http://www.landesbioscience.com/journals/islets/article/24166

Supplementary Material

Ion channels and regulation of insulin secretion in human beta-cells. A computational systems analysis

L.E. Fridlyand[1], D. A. Jacobson[2] and L. H. Philipson[1]

[1] Department of Medicine, University of Chicago, Chicago, IL, USA

[2] Deparment of Molecular Physiology and Biophysics, Vanderbilt University, Nashville, TN, USA

Appendix 1.

Computational model of membrane potential modulation of insulin secretion.

A schematic diagram of the biochemical steps, Ca^{2+} handling, channels and mechanisms of IS regulation in β-cell is presented in Fig 1 in text. The data used to fit the computational model in our study were taken were possible from isolated human β-cells and islets. Since human pancreatic β-cells remain incompletely understood, there remain gaps in any completely β-cell specific data set. For the purpose of making a convenient model we have chosen plausible suggestions of mechanisms of regulation and parameters from rodent β-cells or other cell types to close the gaps.

1. Channels and their mathematical description

The electrophysiological behavior of a single β-cell can be described with the following current balance differential equation

$$-C_m \frac{dV_P}{dt} = I_{Na} + I_{CaL} + I_{CaP} + I_{CaT} + I_{PCa} + I_{KDr} + I_{KCab} + I_{KCa} + I_{Kher} + I_{KATP} + I_{Nab} \quad (1)$$

where V_p is the plasma membrane potential, t is time, C_m is the whole-cell membrane capacitance, I_{Na} is the voltage-gated Na^+ current, I_{CaL} and I_{CaP} are high-voltage-activated "L- and P/Q-type" Ca^{2+} currents, I_{CaT} is the low-voltage-activated "T-type" Ca^{2+} current, I_{PCa} is the plasma membrane Ca^{2+}-pump current, I_{KDr} is the rapid delayed-rectifier K^+ current, I_{KCab} is the Ca^{2+} and high voltage-activated K^+ (BK-like) current, I_{KCa} is the Ca^{2+} activated K^+ (SK-like) current, I_{Kher} is the human-ERG K^+ channel current, I_{KATP} is the ATP-sensitive K^+ channel current and I_{Nab} is the Na^+ background current (Fig. 1 in text). Mathematical description of currents is represented in Appendix 2.

2. Mathematical description of Ca^{2+} dynamics

Ca^{2+} enters into cells through Ca^{2+} channels and is removed by Ca^{2+} pumps and exchangers. Ca^{2+} handling can also include ER and mitochondrial sequestration. Including only fluxes through Ca^{2+}

channels and Ca^{2+} pumps on PM, the equations for free cytoplasmic Ca^{2+} ($[Ca^{2+}]_c$) dynamics can be written as follows:

$$\frac{d[Ca^{2+}]_c}{dt} = \frac{f_{ci}\,(-I_{CaL} - I_{CaT} - I_{CaP} - 2\,I_{PCa})}{2\,F\,V_c} - k_{sg}\,[Ca^{2+}]_c \qquad (2)$$

where f_{ci} is the fraction of free Ca^{2+} in cytoplasm, F is Faraday's constant, V_c is the effective volumes of the cytosolic compartment, and k_{sg} is a coefficient of the sequestration rate of $[Ca^{2+}]_c$.

However, detailed data on Ca^{2+} dynamics during one spike in human islets is lacking, so we used the coefficients we employed for mouse islets[1] (Table S1).

3. Insulin release

We model the electrophysiological events inside one cell and also describe granule exocytosis for one cell. We represent the long-term insulin release in its simplest form as the dependence both on Ca^{2+} influx through specific non-L-type Ca^{2+} channels and $[Ca^{2+}]_c$ as in our models for "immediate fusion" of insulin granules (see for details[2]) and glucagon secretion.[3] Then a rate of relative IS for one cell can be written as

$$f_{is} = f_{VCa}\, f_{iCa} + k_{re} \qquad (3)$$

$$f_{VCa} = (-k_{ci}\, I_{CaP}/F) \qquad (4)$$

$$f_{iCa} = [Ca^{2+}]_c^{\,hiCa}/(K_{iCa}^{\,hiCa} + [Ca^{2+}]_c^{\,hiCa}) \qquad (5)$$

where f_{is} is the rate of exocytosis in one cell; f_{VCa} is the activation function of non-L-type Ca^{2+} channels, where k_{ci} is the stoichiometric coefficient and I_{CaP}/F is the Ca^{2+} influx through specific VGCCs (P/Q-type Ca^{2+} channels in this work); f_{iCa} is the calcium potentiating factor, where K_{iCa} is the half-maximum Ca^{2+} activation constant and hiCa is the Hill coefficient and k_{re} is the rate coefficient for insulin production under resting conditions (in hyperpolarized cells).

To express the experimentally measured rates of long-term IS we should take into account all β-cells in all islets. For simplification we propose that insulin release occurs in numerous β-cells which have similar properties. For example, in a hypothetical perfusion experiment where one islet

is localized in a perfusion chamber, the insulin concentration in media surrounding this islet and the rate of insulin release from this chamber can be written as in article[3]

$$d\,[In]_s / dt = f_{si}\, N_i/V_{pi} - k_{pi}\,[In]_s \quad (6)$$

$$I_s = k_{si}\, k_{pi}\,[In]_s \quad (7)$$

where $[In]_s$ is the relative insulin concentration in medium, f_{si} is the rate of exocytosis in one cell, N_i is the amount of β-cells in one islet, V_{pi} is the volume of the chamber, k_{pi} is the perfusion coefficient, I_{sr} is the relative insulin secretion rate in the perfusion experiment, k_{si} is the scaling coefficient.

Human islets contain a substantially higher proportion of α- and δ-cells than rodent islets.[4-5] Estimated that an "average" islet has about 1000 cells[6] we suggested that the number of β-cells in one islet (coefficient N_i in Eq. 6) is about 600. We have used relative units for our comparative simulations of $[In]_s$ and IS and fit the coefficients for insulin release in Table S1 suggesting that mean relative insulin concentration in chamber and relative I_s are about 1 at high glucose levels in our hypothetical perfusion experiment (see Fig. 3 in text).

4. Computational model

We have constructed the computational model of insulin secretion in human β-cells as the complex of the differential equations for the regulation of PM potential (Eq. 1) , Ca^{2+} handling (Eq.2), $[In]_s$ (Eq. 6) and the voltage-dependent gating variables for channels (see Appendix 2). The influence of glucose was modeled as the changes in ATP/ADP ratio that determines K_{ATP} channel opening.

Precise determination of the model coefficients is limited due to a lack of adequately experimental data. Therefore, the model parameters were evaluated from the literature when possible and were also found by fitting a set of known experimental data as an important reality-test. Equations and parameter values (Table S1 and S2) contain all the information necessary to carry out the simulations presented in this paper and are pointed out in the text as a simulation at basal levels. In some cases, when the values of parameters differed from those at basal level the values assigned are noted in the text or in the corresponding figure legends. To calculate persistent

cellular parameters, the model was allowed to run up to steady values without changes in coefficients.

The units, except where indicated otherwise, are: time in milliseconds (ms), voltage in millivolts (mV), concentration in micromoles/liter (μM), current in femtoamperes (fA), conductance in picosiemens (pS), capacitance in femtofarads (fF).

Numerical integration was carried out using standard numerical methods. Simulations were performed using the software environment "Virtual Cell"[7]. This model is available for direct simulation on the website "Virtual Cell" (www.nrcam.uchc.edu) in "MathModel Database" on the "math workspace" in the library "Fridlyand" with the name "Human_Beta_cell". Visualization and graphical analysis were performed using "Excel".

TABLE S1. Cell and membrane current parameters

Parameter	Definition	Value	Units	Equation	Reference
C_m	Membrane capacitance	9,990	fF	1	[8]
V_c	Cytosol volume	0.764	pL	2	[9]
f_{ci}	Fraction of free Ca^{2+} in cytoplasm	0.005	Ul	2	f
F	Faraday constant	96,487	C/mol	2	Physical constant
k_{sg}	Coefficient of the sequestration rate of $[Ca^{2+}]_c$	0.00001	ms^{-1}	2	[9]
k_{re}	Coefficient of relative insulin production in rest conditions	0.00073	ms^{-1}	3	f
k_{ci}	Stoichiometric coefficient	2	Ul	4	f
K_{iCa}	Half-maximum Ca^{2+} activation constant	0.2	μM	5	f
h_{iCa}	Hill coefficient	2	Ul	5	f
N_i	Amount of β-cells in one islet	600	Ul	6	f
V_{pi}	Relative volume of the chamber	45000	Ul	6	f
k_{pi}	Perfusion coefficient.	0.0001	ms^{-1}	7	f
k_{si}	Scaling coefficient	10000	Ul	7	f

f, adjusted to fit the experimental values; Ul, unitless

Appendix 2.

Mathematical modeling of ion channels

This section details the equations and parameters utilized in the simulations of human β-cell action potential. A conventional Hodgkin-Huxley-type model was used for voltage-gated Ca^{2+}, Na^+ and K^+ channels as it was used in our previous model that described spike activity in mouse β-cells.[1] Boltzman-type equations are employed for steady-state activation and inactivation functions. Coefficients used in the model were either adopted from previous models[1, 9-11] or are described here (Tables S1 and S2). While some aspects of human β–cell physiology and pharmacology have been reported, many quantities, like the measurement of the individual K^+, Na^+ and Ca^{2+} channel contributions to the overall V_p responses during AP generation, the time constants for channel's parameters and others have not been determined experimentally. The parameters for which there are no specific experimental data were chosen during preliminary simulations to produce a close fit to experimentally observed I-V relations for corresponding currents and to reproduce reasonable picture of AP firing in different experimental conditions (see Secs. 4-7 in text for simulations). However, all parameters and constants were fitted to be in their physiological ranges.

1. Voltage-gated Na^+ current (I_{Na}) (Figure S1)

The classic formulation for the I_{Na} current assumes that the Na^+ conductance is controlled by the product of the activation variable (d_{Na}) and the fast inactivation gating variable (f_{Na})[12] that we also used. Coefficients for steady-state activation and inactivation variable curves were fitted to have a bell-shaped peak current voltage dependence with activation near -30 mV and the maximal height at 0 mV for of human Na^+ channels in β-cells[8, 13-14] (Fig. S1C and Table S2). Values of the time constants for the gating variable have not been characterized, so we used approximations based on current decay data[8] (Table S2). Additionally, the voltage-independent coefficient (k_{Nar}, Eq. A1) was included to analyze a role for hypothetical persistent Na^+ current (see discussion in Sec. 6.2). This coefficient was accepted as zero at basal set of coefficients in Table S2. Then

$$I_{Na} = g_{mNa} (d_{Na}^3 f_{Na} + k_{Nar}) (V_P - E_{Na}) \quad (A1)$$

$$\frac{d\, d_{Na}}{dt} = \frac{d_{Nai} - d_{Na}}{\tau_{dNa}} \quad \text{(A2)}$$

$$d_{Nai} = \frac{1}{1 + \exp[(V_{dNa} - V_P)/ k_{dNa}]} \quad \text{(A3)}$$

$$\frac{d\, f_{Na}}{dt} = \frac{f_{Nai} - f_{Na}}{\tau_{fNa}} \quad \text{(A4)}$$

$$f_{Nai} = \frac{1}{1 + \exp[-(V_{fNa} - V_P)/ k_{fNa}]} \quad \text{(A5)}$$

Our simulations are consistent with the experimental finding from[8] (see Fig. S1).

2. L-type Ca^{2+} current (I_{CaL}) (Figure S2)

I_{CaL} was modeled similarly as in our model for mouse β-cell[1] with both fast and slow inactivation gating variables (Fig. S2 and Eqs. A6-A13). Due to a lack of experimental data for activation and inactivation time constants for I_{CaL} in human β-cells, the formulations from models [1] based on rodent experiments were also used.

$$I_{CaL} = g_{mCaL}\, d_{CaL}\, f_{1CaL}\, f_{2CaL}\, (V_P - E_{Ca}) \quad \text{(A6)}$$

$$\frac{d\, d_{CaL}}{dt} = \frac{d_{CaLi} - d_{CaL}}{\tau_{dCaL}} \quad \text{(A7)}$$

$$d_{CaLi} = \frac{1}{1 + \exp[(-V_{dCaL} - V_P)/k_{dCaL}]} \quad \text{(A8)}$$

$$\tau_{dCaL} = 2.2\text{-}1.79*\exp\text{-}[(V_p - 9.7)/70.2]^2 \quad \text{(A9)}$$

$$\frac{d\, f_{1CaL}}{dt} = \frac{f_{1CaLi} - f_{1CaL}}{\tau_{f1CaL}} \quad \text{(A10)}$$

$$f_{1CaLi} = \frac{1}{1 + \exp[-(V_{f1CaL} - V_P)/k_{f1CaL}]} \quad \text{(A11)}$$

$$\frac{d f_{2CaL}}{dt} = \frac{f_{2CaLi} - f_{2CaL}}{\tau_{f2CaL}} \quad \text{(A12)}$$

$$f_{2CaLi} = f_{1CaLi} \quad \text{(A13)}$$

3. P/Q-type Ca^{2+} current (I_{CaP}) (Figure S2)

High-voltage-activated P/Q Ca^{2+} current (I_{CaP}) was also found in human β-cells that posses the fast activated and, apparently, only one slow inactivated voltage-gated variable.[8] There were no data available on voltage-dependence for I_{CaP} activation and inactivation and corresponding time constants in human β-cells so the coefficients from model for I_{CaL} were partially employed (Eqs. A14-A18). However, the coefficients for the steady-state activation variable curve were fitted to obtain a bell-shaped voltage dependence with activation near -20 mV and a maximal peak current close to 0 mV, as previously reported[8] (see Fig. S2).

$$I_{CaP} = g_{mCaP}\, d_{CaP}\, f_{CaP}\, (V_P - E_{Ca}) \quad \text{(A14)}$$

$$\frac{d d_{CaP}}{dt} = \frac{d_{CaPi} - d_{CaP}}{\tau_{dCaP}} \quad \text{(A15)}$$

$$d_{CaPi} = \frac{1}{1 + \exp[(-V_{dCaP} - V_p)/k_{dCaP}]} \quad \text{(A16)}$$

$$\frac{d f_{CaP}}{dt} = \frac{f_{CaPi} - f_{CaP}}{\tau_{fCaP}} \quad \text{(A17)}$$

$$f_{CaPi} = \frac{1}{1 + \exp[-(V_{fCaP} - V_P)/k_{fCaP}]} \quad \text{(A18)}$$

4. T-type Ca^{2+} current (I_{CaT}) (Figure S3)

The activation and inactivation of the I_{CaT} current was defined similarly to the P-type current. Coefficients for the steady-state activation variable curve were fitted to obtain a bell-shaped voltage dependence with an activation of above -60 mV and a maximal peak current between -40 mV and -30 mV, as previously reported[8] (see Fig. S3).

$$I_{CaT} = g_{mCaT}\, d_{CaT}\, f_{CaT}\, (V_P - E_{Ca}) \quad \text{(A19)}$$

$$\frac{d\, d_{CaT}}{dt} = \frac{d_{CaTi} - d_{CaT}}{\tau_{dCaT}} \quad \text{(A20)}$$

$$d_{CaTi} = \frac{1}{1 + \exp[(V_{dCaT} - V_P)/ k_{dCaT}]} \quad \text{(A21)}$$

$$\frac{d\, f_{CaT}}{dt} = \frac{f_{CaTi} - f_{CaT}}{\tau_{fCaT}} \quad \text{(A22)}$$

$$f_{CaT} = f_{CaTi} = \frac{1}{1 + \exp[-(V_{fCaT} - V_P)/k_{fCaT}]} \quad \text{(A23)}$$

5. Delayed Rectifier K^+ current (I_{KDr}) (Figure S4A)

Delayed Rectifier K^+ current activates at membrane potential near -30 mV and then increased with the applied voltage, an inactivation was negligible during at least 200 ms depolarization.[15] The conventional Hodgkin-Huxley-type model for I_{KDr} and some corresponding coefficients was used from our previous mouse β-cell model.[1]

$$I_{KDr} = g_{mDKr}\, d_{Kr}^{\,2}\, f_{Kr}\, (V_P - E_K), \quad \text{(A24)}$$

$$\frac{d\, d_{Kr}}{dt} = \frac{d_{Kri} - d_{Kr}}{\tau_{dKr}} \quad \text{(A25)}$$

$$d_{Kri} = \frac{1}{1 + \exp[(V_{DKr} - V_P)/ k_{dKr}]} \quad \text{(A26)}$$

$$f_{Kri} = 1 \quad \text{(A27)}$$

6. Voltage-gaged Ca^{2+}-activated K^+ current (I_{KCaB}) (Figure S4B)

The sensitivity of BK channels to Ca^{2+} was modeled as previously.[11, 16] Here we have also suggested that Ca^{2+} concentration is high in microdomains surrounding BK channels when they are functioning during a spike period (see Sec. 5.2). However, the voltage dependence of the activation and inactivation gating variables and time constants were not measured and several published models[11, 16] cannot accurately describe the bell-shaped voltage-dependence seen experimentally.[8] For this reason, the coefficients for BK channels were fit to obtain an initial increase in peak amplitude voltage dependence from -40 mV to 20 mV to approximate the published initial part of the peak amplitude (see Fig. 2D,[8]). This is a sufficient approximation for our model where the simulated maximal peak voltage during spikes was less than 20 mV.

$$I_{KCaB} = g_{mKCaB}\, d_{KCaB}^{\,2}\, f_{KCaB}\, (V_P - E_K), \quad \text{(A28)}$$

where

$$\frac{d\, d_{KCaB}}{dt} = \frac{d_{KCaBi} - d_{KCaB}}{\tau_{dKCaB}} \quad \text{(A29)}$$

$$d_{KCaBi} = \frac{1}{1 + \exp[(V_{dKCaB} - V_P)/\, k_{dKCaB}]} \quad \text{(A30)}$$

where

$$V_{dKCaB} = V_{BKo} - k_{shift} \ln ([Ca^{2+}]_c / k_{CaBK}) \quad \text{(A31)}$$

$$\frac{d\, f_{KCaB}}{dt} = \frac{f_{KCaBi} - f_{KCaB}}{\tau_{fKCaB}} \quad \text{(A32)}$$

$$f_{KCaBi} = \frac{1}{1 + \exp[-(V_{fKCaB} - V_P)/\, k_{fKCaB}]} \quad \text{(A33)}$$

7. Human-ERG (HERG) current (I_{Kher})

We modeled this current similarly[10] using a Hodgkin-Huxley-type model with slow activation and deactivation voltage-gated variables:

$$I_{Kher} = g_{mKhe}\, d_{Khe}\, f_{Khe}\, (V_P - E_K), \tag{A34}$$

$$\frac{d\, d_{Khe}}{dt} = \frac{d_{Khei} - d_{Khe}}{\tau_{dKhe}} \tag{A35}$$

$$d_{Khei} = \frac{1}{1 + \exp\,(V_{dKhe} - V_p)\, k_{dKhe}} \tag{A36}$$

$$\frac{d\, f_{Khe}}{dt} = \frac{f_{Khei} - f_{Khe}}{\tau_{fKhe}} \tag{A37}$$

$$f_{Khei} = \frac{1}{1 + \exp[-(V_{fKhe} - V_P)/k_{fKhe}]} \tag{A38}$$

8. Voltage-independent Ca^{2+}-activated K^+ current (I_{KCa})

We included the equation for a calcium-activated K^+ current (I_{KCa}) from our previous model.[1]

$$I_{KCa} = g_{mKCa}\, d_{KCa}\, (V_p - E_K), \tag{A39}$$

where

$$d_{KCa} = \frac{[Ca^{2+}]_c^{\,4}}{[Ca^{2+}]_c^{\,4} + K_{KCa}^{\,4}} \tag{A40}$$

9. ATP-sensitive K^+ channels current (I_{KATP})

For ATP-sensitive K^+ channels current (I_{KATP}) we adopted a kinetic model[1, 9] for the value of whole-cell K_{ATP} channel conductance.

$$I_{KATP} = g_{mKATP}\, O_{KATP}\, (V_P - E_K), \tag{A41}$$

where

$$O_{KATP} = \frac{0.08\,(1 + 2\,[MgADP_f]_c\,/k_{dd}) + 0.89\,([MgADP_f]_c\,/\,k_{dd})^2}{(1 + [MgADP_f]_c\,/\,k_{dd})^2\,(1 + 0.45\,[MgADP_f]_c\,/\,k_{td} + [ATP_f]_c\,/\,k_{tt})} \quad \text{(A42)}$$

$$[MgADP_f]_c = 0.55\,[ADP_f]_c \quad \text{(A43)}$$

where O_{KATP} is the fraction of open K_{ATP} channels, $MgADP_f$ is free Mg-bound ADP, $[ATP_f]_c$ and $[ADP_f]_c$ are free ATP and ADP concentrations in cytoplasm; k_{dd}, k_{td} and k_{tt} are coefficients.

10. Plasma membrane Ca^{2+} pump current (I_{pCa})

The corresponding equation was adapted from previous models.[1, 9]

$$I_{PCa} = P_{mCap}\,\frac{[Ca^{2+}]_c^{\,2}}{[Ca^{2+}]_c^{\,2} + K_{Cap}^{\,2}} \quad \text{(A44)}$$

11. Na^+ background current (I_{Nab})

In addition to the voltage-gated Na^+ current described above, the model contains Na^+ background (leak) current (see Sec. 6.3). We simulated it as previously for mouse β-cell electrical activity (see for details.[1, 9]

$$I_{Nab} = g_{bNa}\,(V_P - E_{Na}) \quad \text{(A45)}$$

TABLE S2. Cell and membrane current parameters (Appendix 2)

Parameter	Definition	Value	Equation	Reference
g_{mNa}	Conductance of I_{Na}	10,000 pS	A1	f
E_{Na}	Reversal potential for Na^+	70 mV	_	[9]
k_{Nar}	Coefficient for persistent Na^+ current	0	_	f
τ_{dNa}	Time constant for d_{Na}	0.1 ms	A2	f
V_{dNa}	Half-activation potential	-30 mV	A3	f
k_{dNa}	Slope of half-activation potential	10 mV	_	f
τ_{fNa}	Time constant for f_{Na}	0.5 ms	A4	f
V_{fNa}	Half-inactivation potential	-42 mV	A5	[8]
k_{fNa}	Slope of half-inactivation potential	6 mV	_	[8]
g_{mCaL}	Conductance for I_{CaL}	2700 pS	A6	f
E_{Ca}	Reversal potential for Ca^{2+} current	100 mV	_	[9]
V_{dCaL}	Half-activation potential	-15 mV	A8	f
k_{dCaL}	Slope of half-activation potential	8 mV	_	f
τ_{f1CaL}	Time constant for f_{1CaL}	6.8 ms	A10	[8]
V_{f1CaL}	Half-inactivation potential	-25 mV	A11	f
k_{f1CaL}	Slope of half-inactivation potential	8 mV	_	[9]
τ_{f2CaL}	Time constant for f_{2L}	65 ms	A124	[8]
g_{mCaP}	Conductance for I_{CaP}	1200 pS	A14	f
τ_{dCaP}	Time constant for d_{CaP}	0.41 ms	A15	f
V_{dCaP}	Half-activation potential	-5 mV	A16	f

k_{dCaP}	Slope of half-activation potential	6 mV	_	f
τ_{fCaP}	Time constant for f_{CaP}	65 ms	A17	f
V_{fCaP}	Half-inactivation potential	-25 mV	A18	f
k_{fCaP}	Slope of half-inactivation potential	8 mV	_	f
g_{mCaT}	Maximum conductance for I_{CaT}	250 pS	A19	f
τ_{dCaT}	Time constant for d_{CaT}	0.41 ms	A20	[8]
V_{dCaT}	Half-activation potential	-50 mV	A21	f
k_{dCaT}	Slope of half-activation potential	6 mV	_	f
τ_{fCaT}	Time constant for f_{CaT}	6.8 ms	A22	[8]
V_{fCaT}	Half-inactivation potential	-64 mV	A23	[8]
k_{fCaT}	Slope of half-inactivation potential	8 mV	_	[8]
g_{mKDr}	Maximum conductance for I_{DKr}	18,000 pS	A24	f
E_K	Reversal potential for K^+ current	-75 mV	_	[9]
τ_{dKr}	Time constant for d_{Kr}	20 ms	A25	f
V_{dKr}	Half-activation potential	-9 mV	A26	[9]
k_{dKr}	Slope of half-activation potential	8 mV	_	f
g_{mKCaB}	Maximum conductance for I_{KCaB}	25,000 pS	A28	f
τ_{dKCaB}	Time constant for d_{KCaB}	1.9 ms	A29	[8]
k_{dKCaB}	Slope of half-activation potential	30 mV	A31	f
K_{CaBK}	Ca^{2+} binding constant for I_{KCaB}	1.5 μM	A31	[11]
V_{BKo}	Constant	0.1 mV	_	[11]
k_{shift}	Voltage-shift constant	18 mV	_	[11]

τ_{fKCaB}	Time constant for f_{KCaB}	22.6 ms	A32	[8]
V_{fKCaB}	Half-inactivation potential	30 mV	A33	f
k_{fKCaB}	Slope of half-inactivation potential	9.2 mV	_	f
g_{mKhe}	Maximum conductance for I_{Kher}	200 pS	A34	f
τ_{dKhe}	Time constant for d_{Khe}	100 ms	A35	[10]
V_{dhe}	Half-activation potential	-30 mV	A36	[10]
k_{dhe}	Slope of half-activation potential	10 mV	_	[10]
τ_{fKhe}	Time constant for f_{Khe}	50 ms	A37	[10]
V_{fhe}	Half-inactivation potential	-42 mV	A38	[10]
k_{fhe}	Slope of half-inactivation potential	17.5 mV	_	[10]
g_{mKCa}	Maximum conductance for I_{KCa}	150 pS	A39	f
K_{KCa}	Affinity constant	0.2 μM	A40	f
g_{mKATP}	Maximum conductance for I_{KATP}	45,000 pS	A41	f
$[ADP_f]_c$	Free ADP concentration in cytoplasm at high glucose level	15 μM	A42	f
$[ATP_f]_c$	Free ATP concentration in cytoplasm	3600 μM	_	f
k_{dd}	Dissociation constant	17 μM	_	[9]
k_{td}	Dissociation constant	26 μM	_	[9]
k_{tt}	Dissociation constant	50 μM	_	[9]
P_{mCap}	Maximum I_{Cap} current	5600 fA	A44	f
K_{Cap}	Half-maximum Ca^{2+} binding constant for I_{Cap}	0.3 μM	_	f
g_{bNa}	Maximum conductance for I_{Nab}	10 pS	A45	f

f, adjusted to fit the experimental values.

Reference List

1. Fridlyand LE, Jacobson DA, Kuznetsov A, Philipson LH. A model of action potentials and fast Ca2+ dynamics in pancreatic beta-cells. Biophys J 2009; 96:3126-39.
2. Fridlyand LE, Philipson LH. Coupling of metabolic, second messenger pathways and insulin granule dynamics in pancreatic beta-cells: a computational analysis. Prog Biophys Mol Biol 2011; 107:293-303.
3. Fridlyand LE, Philipson LH. A computational systems analysis of factors regulating alpha cell glucagon secretion. Islets 2012; 4:262-83.
4. Henquin JC, Rahier J. Pancreatic alpha cell mass in European subjects with type 2 diabetes. Diabetologia 2011; 54:1720-5.
5. Kilimnik G, Jo J, Periwal V, Zielinski MC, Hara M. Quantification of islet size and architecture. Islets 2012; 4:167-72.
6. Rorsman P, Renstrom E. Insulin granule dynamics in pancreatic beta cells. Diabetologia 2003; 46:1029-45.
7. Slepchenko BM, Loew LM. Use of virtual cell in studies of cellular dynamics. Int Rev Cell Mol Biol 2010; 283:1-56.
8. Braun M, Ramracheya R, Bengtsson M, Zhang Q, Karanauskaite J, Partridge C, et al. Voltage-gated ion channels in human pancreatic beta-cells: electrophysiological characterization and role in insulin secretion. Diabetes 2008; 57:1618-28.
9. Fridlyand LE, Tamarina N, Philipson LH. Modeling of Ca2+ flux in pancreatic beta-cells: role of the plasma membrane and intracellular stores. Am J Physiol Endocrinol Metab 2003; 285:E138-54.
10. Pedersen MG. A biophysical model of electrical activity in human beta-cells. Biophys J 2010; 99:3200-7.
11. Tsaneva-Atanasova K, Sherman A, van Goor F, Stojilkovic SS. Mechanism of spontaneous and receptor-controlled electrical activity in pituitary somatotrophs: experiments and theory. J Neurophysiol 2007; 98:131-44.
12. Hodgkin AL, Huxley AF. A quantitative description of membrane current and its application to conduction and excitation in nerve. J Physiol 1952; 117:500-44.
13. Barnett DW, Pressel DM, Misler S. Voltage-dependent Na+ and Ca2+ currents in human pancreatic islet beta-cells: evidence for roles in the generation of action potentials and insulin secretion. Pflugers Arch 1995; 431:272-82.
14. Misler S, Barnett DW, Gillis KD, Pressel DM. Electrophysiology of stimulus-secretion coupling in human beta-cells. Diabetes 1992; 41:1221-8.
15. Dai XQ, Manning Fox JE, Chikvashvili D, Casimir M, Plummer G, Hajmrle C, et al. The voltage-dependent potassium channel subunit Kv2.1 regulates insulin secretion from rodent and human islets independently of its electrical function. Diabetologia 2012; 55:1709-20.
16. Chay TR. On the effect of the intracellular calcium-sensitive K+ channel in the bursting pancreatic beta-cell. Biophys J 1986; 50:765-77.

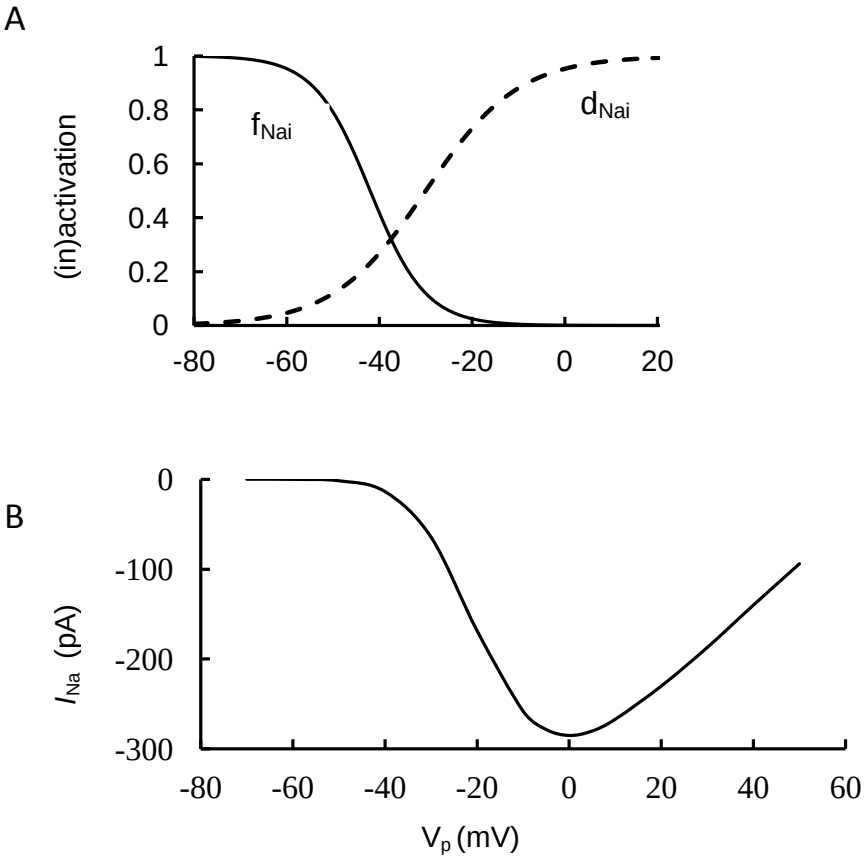

Figure S1. Tetrodotoxin (TTX) sensitive Na^+ current (I_{Na}). A: steady-state activation (— — — d_{Nai}) and inactivation (—— f_{Nai}) functions with parameters as in Table S2. B: Simulated peak *I-V* relationship of I_{Na} obtained from Eqs. A1-A5. Voltage clamp pulses from – 60 mV to 40 mV from a holding potential of -70 mV were simulated to reproduce the results of Fig. 4C from[8].

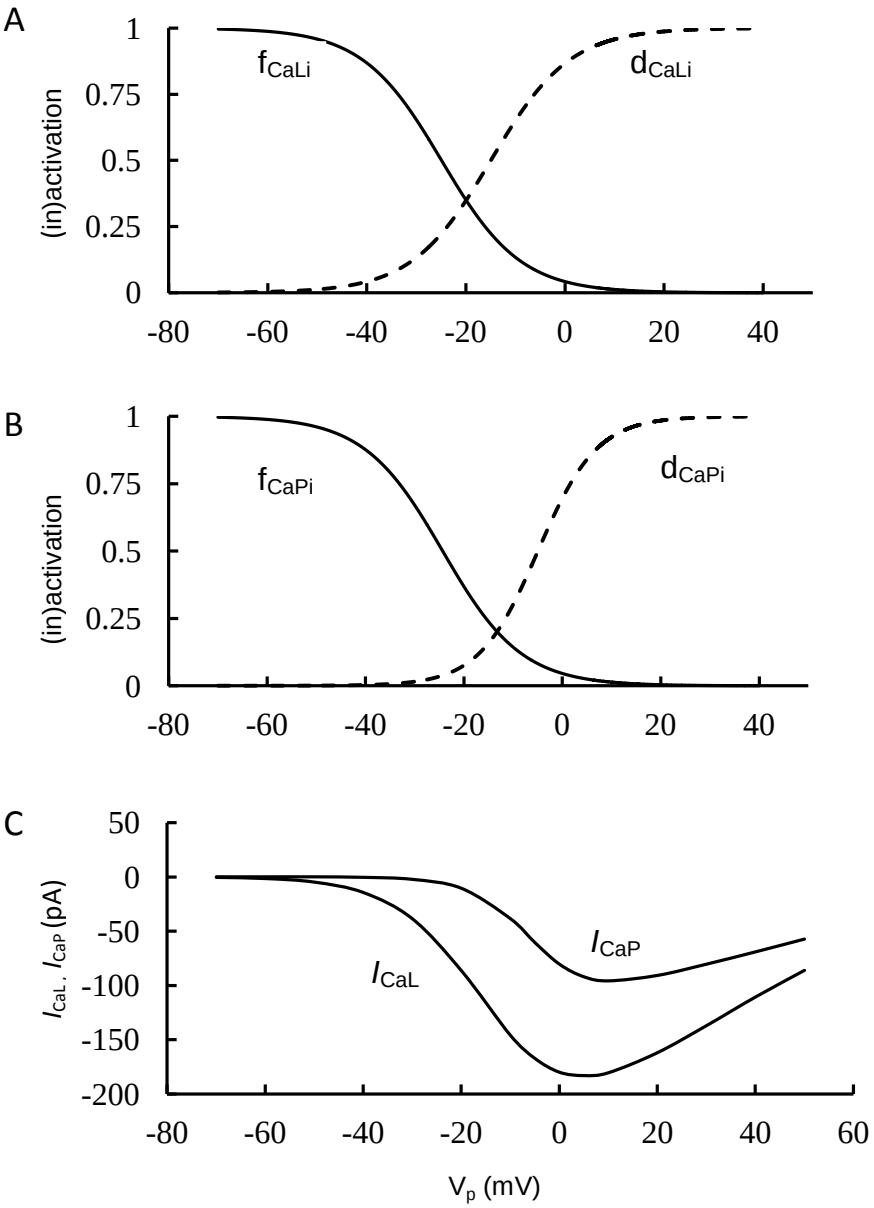

Figure S2. **L and P/Q types Ca^{2+} current (I_{CaL} and (I_{CaP})).** A: A: steady-state activation (— — — d_{CaLi}) and inactivation (—— f_{CaLi}) functions for L-type Ca^{2+} channels with parameters as in Table S2. (Steady-state inactivation function (f_{CaLi}) is similar for fast and slow inactivated voltage-gated variables, see Eq. A13). 2. B: steady-state activation (— — — d_{CaPi}) and (—— f_{CaPi}) inactivation functions for P-type Ca^{2+} channels with parameters as in Table S2. C. Simulated peak *I-V* relationship obtained from Eqs. A6 and A14 with parameters as in Table S2. Voltage clamp pulses from – 60 mV to 50 mV from a holding potential of -70 mV were simulated to reproduce the experimental conditions (see Fig. 5E from[8]).

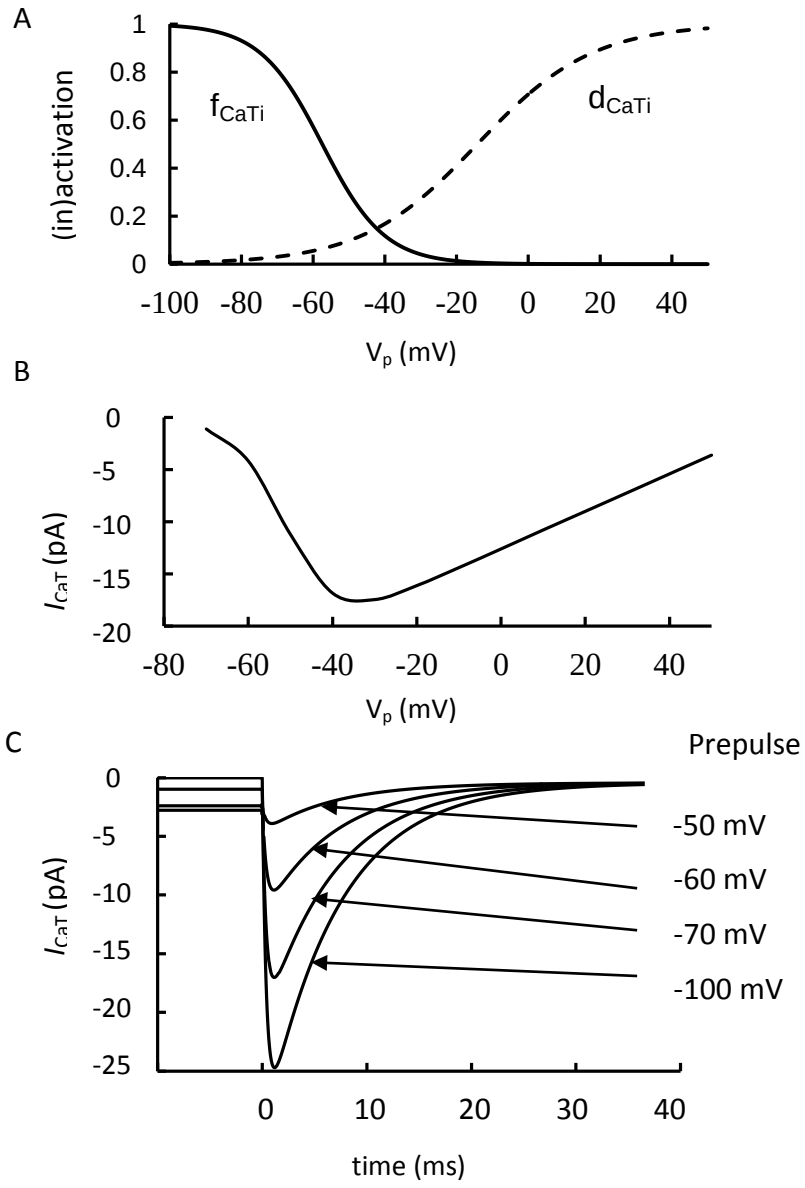

Figure S3. **T-type Ca^{2+} current (I_{CaT}).** A: steady-state activation (d_{CaTi}) and inactivation (f_{CaTi}) functions. B: Simulated peak *I-V* relationship of I_{CaT}. Voltage clamp pulses from – 60 mV to 40 mV (in 10-mV increment) from a holding potential of -70 mV were simulated to reproduce the experimental conditions (see Fig. 5E from[8]). C: simulated I_{CaT} during a test pulse to -30 mV preceded by the prepulses from -100 mV to -40 mV that reproduce the results represented on Fig. 5C from.[8]

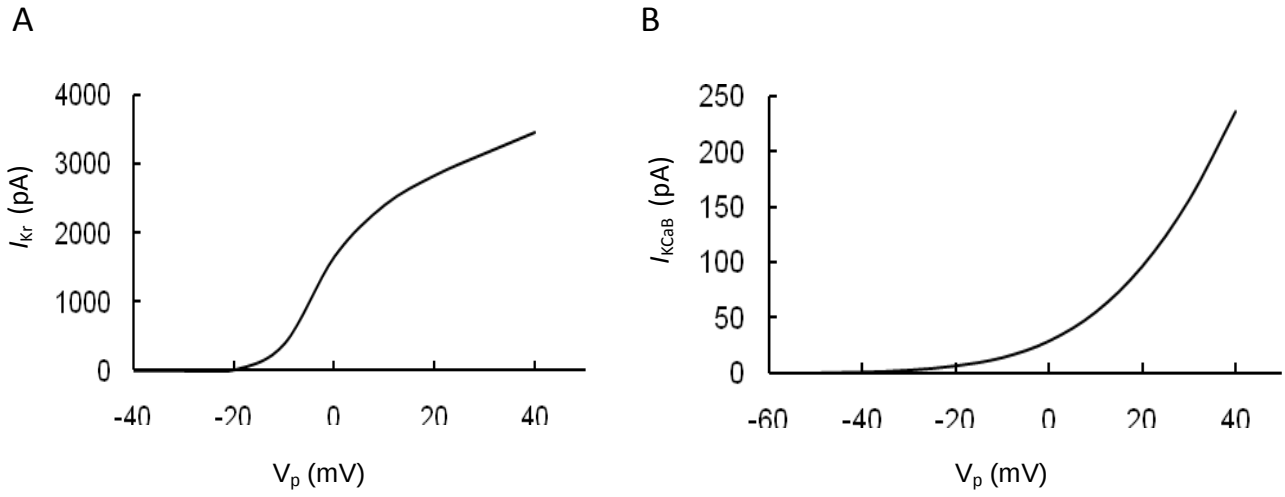

Figure S4. K^+ currents. (A): Simulated peak *I-V* relationship for delayed rectifier K^+ current (I_{KDr}). Voltage clamp pulses (500 ms) from – 60 mV to 50 mV from a holding potential of -70 mV were simulated with parameters as in Table S2 to reproduce the experimental conditions (see Fig. 1 from[8]). (B): BK type K^+ current (I_{KCaB}). Simulated peak *I-V* relationship of I_{KCaB} at $[Ca^{2+}]_c$ = 0.1 µM. Voltage clamp pulses from – 60 mV to 40 mV from a holding potential of -70 mV were simulated to reproduce the results of Fig. 2D from[8]).